(Preprint) AAS 19-815

AEROCAPTURE PERFORMANCE ANALYSIS FOR A NEPTUNE MISSION USING A HERITAGE BLUNT-BODY AEROSHELL

Athul Pradeepkumar Girija[*], Sarag J. Saikia[†], James M. Longuski[‡], Shyam Bhaskaran[§], Matthew S. Smith[¶], and James A. Cutts[‖]

The large navigation and atmospheric uncertainties at Neptune have historically driven the need for a mid-lift-to-drag (L/D) vehicle with $(L/D)_{\max}$ of 0.6–0.8. All planetary entry vehicles flown to date are low-L/D blunt-body aeroshells with L/D less than 0.4. The lack of a heritage mid-L/D aeroshell presents a long pole for Neptune aerocapture, as the development and testing of a new entry vehicle incurs significant cost, risk, and time. Techniques which may allow Neptune aerocapture to be performed using heritage low-L/D blunt-body aeroshells are investigated, and obviate the need for mid-L/D aeroshells. A navigation study is performed to quantify the delivery errors, and a new guidance algorithm with onboard density estimation is developed to accommodate atmospheric uncertainties. Monte Carlo simulation is used to analyze aerocapture performance of a vehicle with $L/D = 0.4$. One hundred percent of the cases captured successfully and show a 99.87% probability of achieving the desired science orbit with a total of 396 m/s propulsive ΔV budget, even with worst-case atmospheric uncertainties.

INTRODUCTION

Aerocapture is a maneuver in which a spacecraft uses aerodynamic drag to decelerate and perform orbit insertion. Neptune's large heliocentric distance and the need to achieve reasonable flight time result in high arrival V_∞ and consequently large orbit insertion ΔV. Propulsive insertion incurs a significant mass penalty due to the large ΔV. Aerocapture at Neptune has been shown to substantially increase delivered mass and allow reduction in flight time compared to propulsive insertion.[1–3] Despite the potential benefits, Uranus and Neptune are the most challenging destinations for performing aerocapture. The large navigation and atmospheric uncertainties drive the need for a vehicle with sufficient control authority to perform aerocapture without the spacecraft risking escape or getting trapped in the atmosphere.[4]

Several mission concepts and technology demonstration flights have proposed the use of aerocapture, but have never been flown.[5–9] Hall et al.[10] showed that aerocapture could enhance missions to

[*]Doctoral Candidate, School of Aeronautics and Astronautics, Purdue University, West Lafayette, IN 47907. AAS Student Member, AIAA Student Member.

[†]Research Assistant Professor, School of Aeronautics and Astronautics, Purdue University, West Lafayette, IN 47907.

[‡]Professor, School of Aeronautics and Astronautics, Purdue University, West Lafayette, IN 47907. AIAA Associate Fellow.

[§]Supervisor, Mission Design and Navigation Section, Jet Propulsion Laboratory, California Institute of Technology, Pasadena, California 91109.

[¶]Navigation Engineer, Mission Design and Navigation Section, Jet Propulsion Laboratory, California Institute of Technology, Pasadena, California 91109.

[‖]Program Manager, Solar System Exploration Directorate, Jet Propulsion Laboratory, California Institute of Technology, Pasadena, CA 91109.

Venus, Mars, Titan, and Uranus and enable some missions to Jupiter, Saturn, and Neptune. Heritage low lift-to-drag ratio ($L/D \leq 0.4$) blunt-body aeroshells and existing thermal protection system (TPS) materials are sufficient for aerocapture at Venus, Mars, and Titan.[4,11–14] Aerocapture studies have historically used a mid lift-to-drag (L/D) vehicle with L/D of 0.6–0.8 to accommodate the large navigation and other uncertainties at Neptune.[15,16] Planetary entry vehicles flown to date are low-L/D vehicles with L/D less than 0.4. The non-availability of a mid-L/D vehicle is a major hindrance to Neptune aerocapture, as development and testing of new entry vehicle is an expensive, time-consuming endeavour with significant programmatic risk. High arrival V_∞ trajectories not considered in previous studies and recent navigation analysis merit investigation of the performance of a low-L/D vehicle for Neptune aerocapture, and is the subject of the present paper.

MISSION DESIGN

A reference interplanetary trajectory is selected to allow a future Cassini style exploration mission of the Neptune system. The process by which the reference trajectory is selected is described in a companion paper*. For a time of flight of 8 years, and a delivered mass requirement of at least 2000 kg in Neptune orbit, preliminary results indicate that the Earth-Jupiter-Neptune trajectory launching in 2031 with a flight time of 7.87 years and C_3 of 111 km^2/s^2 is a promising candidate. Space Launch System (SLS) Block 1B with kick stage is the selected launch vehicle with a launch capability of 6250 kg at the desired C_3. Trajectories to Neptune with flight times less than 13 years are infeasible with propulsive insertion (due to low delivered mass fraction to orbit),[17] and hence the use of aerocapture with SLS allows a 5 year reduction in flight time. The high energy trajectory with a fast arrival V_∞ of 20 km/s enables the use of a heritage blunt body aeroshell with L/D = 0.4 if the Theoretical Corridor Width (TCW) requirement can be lowered to about 1.25 degrees as seen in Fig. 1. The expected peak heat rate is within the capability of state-of-the-art HEEET (Heatshield for Extreme Entry Environment Technology) thermal protection system (TPS). The study emphasizes that these are preliminary estimates from engineering correlations[18] and future higher fidelity studies are required to validate the heating predictions.

Upon arrival near the Neptune sphere of influence, the spacecraft targets the aim point on the B-plane to achieve the desired entry flight-path angle (EFPA) at atmospheric interface and the target orbit inclination.[19] Radiometric and optical navigation is used to guide the spacecraft to achieve the desired trajectory. Trajectory correction maneuvers (TCM) are performed to reduce targeting errors as the spacecraft approaches the Neptune system. On exit from the atmosphere after aerocapture, the spacecraft coasts to an apoapsis of 400,000 km and following a propulsive periapse raise maneuver—establishes the science orbit of 4,000 km x 400,000 km. Two candidate inclinations for the science orbit are: 1) 157° retrograde with respect to Neptune (or 23° prograde) for Triton encounters, and 2) near-polar orbit for interior and magnetic field investigations as used by Juno, and Cassini in the final phase of the mission. The aerocapture guidance algorithm used in present study only considers apoapsis targeting during the aerocapture maneuver and assumes prograde equatorial atmospheric flight to simplify the analysis.

Errors in the B-plane targeting translate to errors in EFPA at the atmospheric entry interface. Knowledge of the B-plane targeting uncertainty is critical to assessing aerocapture mission feasibility using low-L/D aeroshells. If the delivery error is beyond what the vehicle control authority can accommodate, the vehicle guidance control variable is saturated and the guidance algorithm is

*Athul Pradeepkumar Girija et al. "A Unified Framework for Aerocapture Systems Analysis", AAS 19-811, 2019 AAS/AIAA Astrodynamics Specialist Conference, Portland, ME.

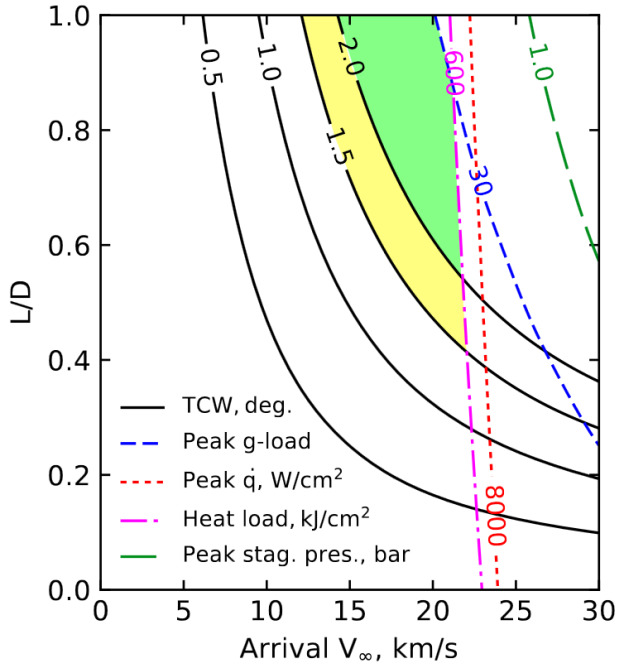

Figure 1. Contours of Theoretical Corridor Width (TCW) and other constraints for Neptune aerocapture as a function of vehicle L/D and interplanetary arrival V_∞. The green regions indicates the feasible design space for TCW requirement of 2.0°. If the TCW requirement is lowered to 1.5° the yellow region becomes feasible in addition to the green region.

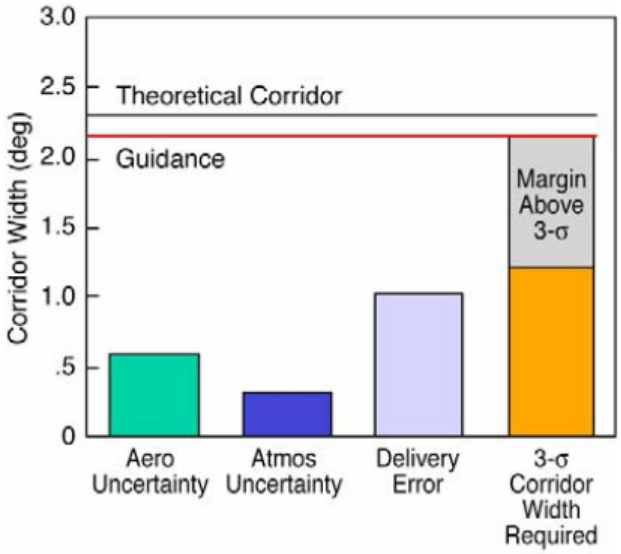

Figure 2. Contribution of various uncertainties and root-sum-squared required corridor width for Neptune aerocapture as estimated by Lockwood et al.[1]

unable to achieve the desired capture orbit. Low-L/D blunt body aeroshells offer less control authority than mid-L/D aeroshells, and can only accommodate smaller EFPA uncertainties compared to mid-L/D aeroshells. Accurate estimation of the navigation uncertainties along with atmospheric and other uncertainties is key to determining if blunt body aeroshells can be used for Neptune aerocapture.

Delivery error from spacecraft approach navigation at Neptune were last quantified in 2004 by Lockwood et al.,[1] and is the dominant uncertainty component as seen in Fig. 2. Improvements in navigation techniques (higher performance camera, refined ephemerides etc.) since the last such study was performed could allow the navigation uncertainty component to be reduced and hence lower the vehicle L/D requirement. Atmospheric uncertainties at Neptune have been modeled in Neptune-Global Reference Atmospheric Model (GRAM), but no improvements are available over the data used by Lockwood et al.[1] Spilker et al.[4] recommends performing opportunistic stellar occultations of Uranus and Neptune to improve the atmospheric models, but also notes that the technique may only provide information at high altitudes and extrapolating to altitudes relevant to aerocapture carries greater uncertainties. A dedicated research program for combined ground-based observations and modeling efforts is required to reduce the atmospheric uncertainties at altitudes relevant to aerocapture. Aerodynamic uncertainties have been quantified for a mid-L/D vehicle at Neptune during the 2004 systems analysis study, but no estimates are available for a low-L/D vehicle. A refined estimate of the delivery error is presented in the present study, along with a discussion of the current state of atmospheric and aerodynamic uncertainties.

UNCERTAINTY QUANTIFICATION

The aerocapture vehicle should have sufficient control authority to compensate for dispersions in approach navigation, atmospheric density dispersions, and aerodynamic uncertainties. Quantification of these uncertainties is essential to evaluate the required vehicle L/D and its performance during the aerocapture maneuver.

Navigation Uncertainty

For the reference interplanetary trajectory, navigation covariance analysis is used to quantify the entry flight-path angle (EFPA) uncertainty at atmospheric entry interface (defined at 1000 km above the 1 bar pressure level). Spacecraft navigation using radiometric tracking and optical navigation (OpNav) is considered. The radiometric data come in three flavors: Doppler, Range, and Delta Differential One-Way Ranging (ΔDOR). The Doppler and range data provide line-of-sight information about the spacecraft, while the ΔDOR measurements enhance plane-of-sky knowledge. OpNav improves spacecraft-body relative knowledge which, for less-studied bodies such as Triton, is imperative. The results are presented for two cases with regard to Neptune's ephemeris covariance: 1) current uncertainty in the ephemeris, and 2) a hypothetical case where the uncertainty in Neptune's ephemeris is reduced by a factor of 100. The justification for the second case was given by William Folkner of the Solar System Dynamics (SSD) group at JPL*. He expects that level of improvement when analyzing recent Neptune observations in the near future. Two candidate optical navigation cameras are considered: 1) a generic camera, and 2) the high performance Long Range Reconnaissance Imager Camera (LORRI) flown on the New Horizons spacecraft. Parameters and assumptions used in the navigation analysis are shown in Table 1.

*Personal Communication

Table 1. Navigation uncertainty analysis parameters and assumptions

Parameter	Values
1. Bodies	• 8 planets • Earth's Moon, Jupiter's Galilean satellites • Triton and Nereid • Spacecraft (6225 kg before aerocapture)
2. Force Model	• Gravity (including relativistic corrections and J_2, J_4 for Neptune)
3. Estimated parameters	• Spacecraft state at epoch • Neptune ephemeris, Triton and Nereid initial state • Impulsive Maneuvers (E-30, E-7, E-5, E-2) • Small burns for repointing (every 3 days) • Neptune pole, barycenter, J_2, J_4, Triton gravitational parameter • Stochastic range biases at stations
4. Assumed sigma / weights	• Maneuvers: 5 cm/s per axis • Small burns: 0.2 mm/s per axis • DDOR: 0.06 ns • Doppler: 0.1 mm/s • Range: 3 m • OpNav: 1 pixel
5. Ephemerides	• Planetary ephemerides: DE430 • Satellite ephemeris: Jup310 and Nep081
6. OpNav schedule	• Triton observations begin E-60 days • Support approach maneuvers and ephemeris updates • Analysis for 3 pictures / day
7. Radiometric tracking schedule	• Doppler/Range (3×8 hrs/week) • ΔDOR (2 pairs / week)
8. Camera specifications	• Camera - iFoV:60 µrad, FoV:122 mrad, focal length: 500 mm • LORRI - iFoV:5 µrad, FoV:5 mrad, focal length: 2,619 mm • iFoV = instantaneous Field of View, FoV = Field of View
9. Maneuvers	• Performed 2 days after Data Cut Off (DCO).

The 1σ entry flight path angle uncertainty for various cases considered in the study are shown in Tables 2 and 3. SMAA, SMIA, and B refer to the 1σ semi-major, semi-minor axis of the B-plane ellipse, and the magnitude of the B-plane aim point vector respectively. For the selected interplanetary trajectory with arrival V_∞ = 20 km/s, a vehicle with L/D = 0.4 entering prograde near the equator results in TCW $\approx 1.25°$. If the $\pm 3\sigma$ navigation uncertainty alone exceeds the TCW, atmospheric and aerodynamic uncertainties cannot be accommodated. Preliminary simulations indicated the 1σ delivery error cannot exceed 0.2° if blunt body aeroshells are used for the reference interplanetary trajectory. Table 2 shows that radiometric tracking alone (i.e. without OpNav) cannot achieve the desired delivery accuracy. Optical navigation using a generic camera with specifications listed in Tab. 1 along with radiometric navigation is also unable to achieve the desired targeting accuracy. LORRI significantly lowers the delivery error, and Data Cut Off (DCO) at E-07 and E-04 days results in delivery errors low enough that blunt body aeroshells are potentially feasible (highlighted in green). E-07 refers to 7 days prior to atmospheric entry. For the hypothetical case with a hundred fold improvement in the Neptune ephemeris shown in Table 3, E-04 DCO is able to achieve the

desired accuracy, but is seen to be larger than the case without the ephemeris improvement. The reason for the small increase when using the scaled covariance for the improved ephemeris is due to noise sources which we considered in the study but were not estimated. Some of the errors could be getting magnified when the data noise is tightly constrained, and the source of this behaviour could not be isolated at the level of the present study. In a real mission scenario, it would be informative to investigate the source of this behaviour.

Results using the current Neptune ephemeris and LORRI is an improvement over the previous estimate in literature which was $\pm 0.17^\circ$ (1σ).[1] The smaller delivery error lowers the TCW requirement and hence the required L/D as shown in Fig. 1. The results represent a preliminary assessment of the delivery uncertainties. Sources of error sources not considered in the study may inflate these uncertainties to some degree. These include but are not limited to: 1) non-gravitational forces (solar radiation pressure, Neptune albedo, Neptune atmosphere), 2) spacecraft noise, and 3) data noise (eg: OpNav data noise as the spacecraft approaches the Neptune system). Future studies with improved spacecraft system definition, can improve the estimation of delivery uncertainty.

Table 2. 1σ EFPA uncertainty using current Neptune ephemeris. Rows highlighted in green indicate EFPA uncertainties low enough that low-L/D aeroshells are potentially feasible.

	Only radiometric tracking, no OpNav		
DCO (days)	B-plane ellipse SMAA × SMIA (km)	B (km)	1σ EFPA error (degrees)
E - 09	328.8 × 255.3	272.9	1.78
E - 07	327.5 × 254.2	271.3	1.77
E - 04	325.1 × 253.3	270.3	1.76
	With radiometric tracking and OpNav (Generic camera)		
E - 09	170.3 × 160.3	162.9	1.06
E - 07	151.5 × 144.1	146.3	0.95
E - 04	116.5 × 113.5	114.4	0.74
	With radiometric tracking and OpNav (LORRI)		
E - 09	39.8 × 35.4	39.2	0.26
E - 07	30.5 × 26.9	30.1	0.20
E - 04	17.6 × 14.6	17.1	0.11

Table 3. 1σ entry flight-path angle (EFPA) uncertainty using 100-fold improvement in Neptune ephemeris

	Only radiometric tracking, no OpNav		
DCO (days)	B-plane ellipse SMAA × SMIA (km)	B (km)	1σ EFPA error (degrees)
E - 09	101.7 × 70.0	100.7	0.65
E - 07	97.8 × 64.0	96.3	0.63
E - 04	94.7 × 51.2	92.3	0.60
	With radiometric tracking and OpNav (Generic camera)		
E - 09	100.3 × 68.1	99.2	0.65
E - 07	96.1 × 61.8	94.3	0.61
E - 04	91.6 × 48.5	88.8	0.58
	With radiometric tracking and OpNav (LORRI)		
E - 09	50.5 × 35.6	48.4	0.31
E - 07	39.8 × 27.2	37.7	0.25
E - 04	25.0 × 14.8	23.1	0.15

Atmospheric Uncertainty

The large heliocentric distance presents a challenge to accurate measurement of Neptune's atmospheric characteristics. The Voyager 2 spacecraft remains the only spacecraft to provide a glimpse of the Neptune atmospheric profile during its flyby in 1989.[4,20] Despite the limited data and the uncertainties in measurements, NASA has developed the Neptune-GRAM (Global Reference Atmosphere Model). GRAMs are engineering level models for planetary atmospheres, and are widely used for systems design and performance analysis of flight trajectories.[21,22] The atmosphere model implemented in Neptune-GRAM is based on the data from Voyager 2 radio science experiment, infrared interferometer-spectrometer (IRIS), and ultraviolet spectrometer (UVS) instrument.[23] Neptune-GRAM provides the density, temperature, pressure, winds and chemical composition as a function of altitude, latitude, longitude, season, and local time. The model accounts for: 1) uncertainty in analysis of Voyager data, 2) latitudinal variations in the atmospheric structure, and 3) temporal changes due to seasonal and diurnal variations.[24]

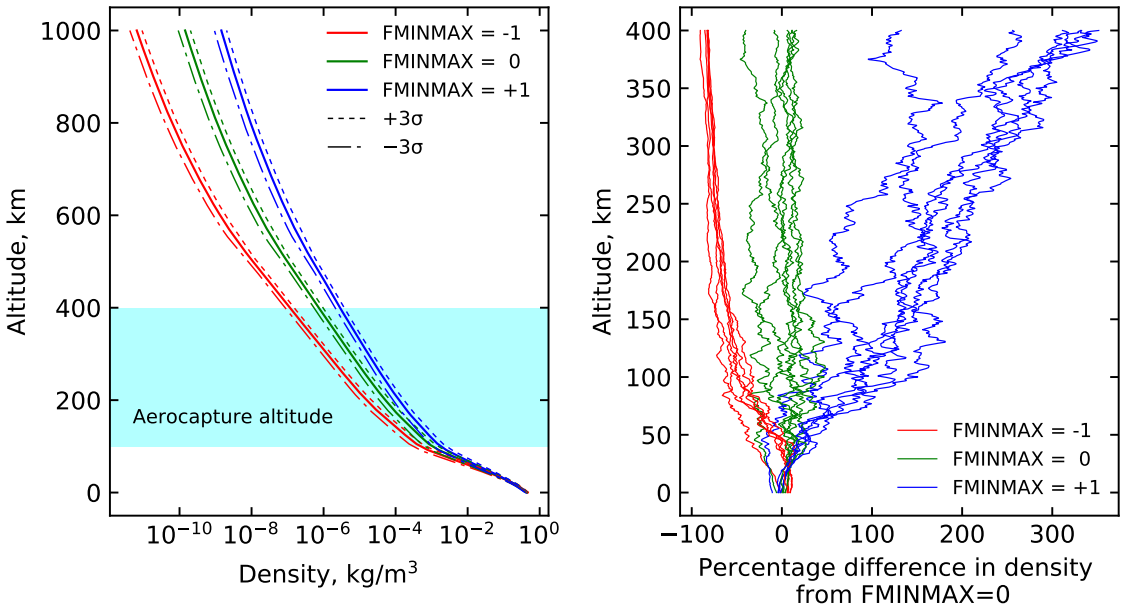

Figure 3. (Left): Mean density profile variations from Neptune-GRAM by varying Fminmax from -1 to +1 and $\pm 3\sigma$ uncertainties for the mean profiles. (Right): Sample of random perturbed density profiles from Neptune-GRAM for different values of Fminmax. High frequency content can significantly alter the density profile from the mean value.[1,23]

Neptune-GRAM uses a single input parameter "Fminmax" to account for uncertainty and variability of the mean density profile. Fminmax = -1 corresponds to the minimum mean density and Fminmax = +1 corresponds to the maximum mean density as shown in Fig. 3. Neptune-GRAM also provides the expected $\pm 3\sigma$ variation of the mean profile about the selected Fminmax value as shown in Fig. 3. The full range of Fminmax along with the 3σ dispersion is expected to cover the worst-case uncertainty in mean density profile. For aerocapture at Neptune, knowledge of the density profile uncertainty is most important in the altitude range 100 km to 400 km which is referred to as the aerocapture altitude range. Aerodynamic forces are negligible above 400 km and the minimum altitude during the aerocapture maneuver is well above 100 km for a wide range of

vehicle L/D and arrival V_∞. Neptune-GRAM also provides high frequency density perturbations superposed on the mean profiles to account for random variations expected in the atmosphere as seen in Fig. 3. The parameter "rpscale" controls the high frequency variability of the atmospheric density and ranges from 0 to 2, with 0 indicating no perturbations and 2 indicating the highest perturbation amplitude. Previous studies a nominal value of rpscale = 1.0, and lower values such as 0.5 indicate lower high frequency content. Previous studies have recommended using a smaller range of Fminmax depending on the arrival season and entry latitude instead of the full range. Lockwood et al.[1] used $0.60 \leq$ Fminmax ≤ 0.93 for an aerocapture vehicle flying in low latitudes in the season corresponding to the arrival time. The present study uses the full range of Fminmax from -1 to +1 as a conservative estimate of the atmospheric uncertainties.

Better knowledge of the atmosphere from ground based observations and modeling may reduce the atmospheric variability both in terms of mean profile and high frequency content. It is possible that existing observations when combined with global circulation models could constrain the range of Fminmax depending on the arrival season, and is worth further investigation. The present study investigates a novel approach called a pathfinder probe recommended by Spilker et al.[4] An entry probe enters the atmosphere several weeks ahead of the main aerocapture vehicle and relays the in-situ atmospheric density data. The aerocapture vehicle performs a trajectory correction maneuver to optimize the entry flight path angle, and is discussed in more detail in the pathfinder probe section.

Aerodynamics Uncertainty

The vehicle aerodynamic control authority is quantified by the hypersonic trim lift-to-drag ratio $(L/D)_{\text{trim}}$ at the nominal angle of attack for bank angle modulation. Ablation of the TPS material during aerocapture, shape changes, and mass imbalances translate into uncertainty in the achievable vehicle L/D. Quantification of aerodynamics uncertainties is important for aerocapture, but is outside the scope of the present work. Previous studies addressing Titan aerocapture using a low-L/D blunt-body aeroshell have estimated a 19% uncertainty in $(L/D)_{\text{trim}}$.[13] The present study uses a 10% 3σ dispersion about the nominal $(L/D)_{\text{trim}}$ as a representative estimate. Entry at Neptune presents a significantly more severe aerothermal environment than at Titan due to the higher entry speed and the H_2-He atmosphere resulting in substantial TPS ablation. Future studies will quantify the aerodynamics uncertainties for a Neptune aerocapture vehicle using CFD and other codes prediction of TPS ablation during the aerocapture maneuver.

GUIDANCE SCHEME

The objective of the aerocapture guidance algorithm is to guide the vehicle from the entry interface through atmospheric flight such that a desired set of terminal conditions are achieved when the vehicle exits the atmosphere. The desired terminal conditions at atmospheric exit allows the spacecraft to achieve the target apoapsis and inclination. The present work uses bank angle modulation as the control method. Bank angle modulation uses an aeroshell which provides lift from offsetting the center of gravity with respect to the symmetry axis. The lift vector is rotated around the velocity vector by banking the vehicle and the bank angle is the sole control variable. Bank angle modulation has been successfully used on entry vehicles such as Apollo and the Mars Science Laboratory (MSL) and is considered a high-heritage flight control technique for low-L/D blunt body aeroshells.[25,26] The guidance scheme used in the present work is a derivative of the Analytical Predictor-Corrector developed by Cerimele and Gamble.[27] The guidance consists of two phases: 1) the equilibrium glide phase, and 2) the exit phase as shown in Fig. 4. In the equilibrium glide

phase, the vehicle attempts to maintain equilibrium glide condition i.e. altitude acceleration $\ddot{h} = 0$. The bank angle command δ_{CMD} during the equilibrium glide phase is computed as

$$\cos\delta_{\text{CMD}} = \cos\delta_{\text{eq. gl.}} - G_{\dot{h}}\dot{h} + G_{\bar{q}}\left(\frac{\bar{q} - \bar{q}_{\text{ref}}}{\bar{q}}\right) \tag{1}$$

where $\cos\delta_{\text{eq. gl.}}$ is the calculated equilibrium glide bank angle to which increments are added, and is given by

$$\cos\delta_{\text{eq. gl.}} = \frac{mg}{C_L\bar{q}S}\left(1 - \frac{v^2}{gr}\right) \tag{2}$$

where, m is the vehicle mass, g is the local gravitational acceleration, C_L is the vehicle lift coefficient, $\bar{q}$ is the dynamic pressure, S is the aerodynamic reference area, v is the atmosphere relative speed, and r is the radial distance from the center of the planet. $G_{\dot{h}}$ and $G_{\bar{q}}$ refer to the gain parameters and are chosen based on the method developed by Cerimele and Gamble. The reference dynamic pressure $\bar{q}_{\text{ref}}$ is computed as

$$\bar{q}_{\text{ref}} = -\frac{mg}{0.75C_LS}\left(1 - \frac{v^2}{gr}\right) \tag{3}$$

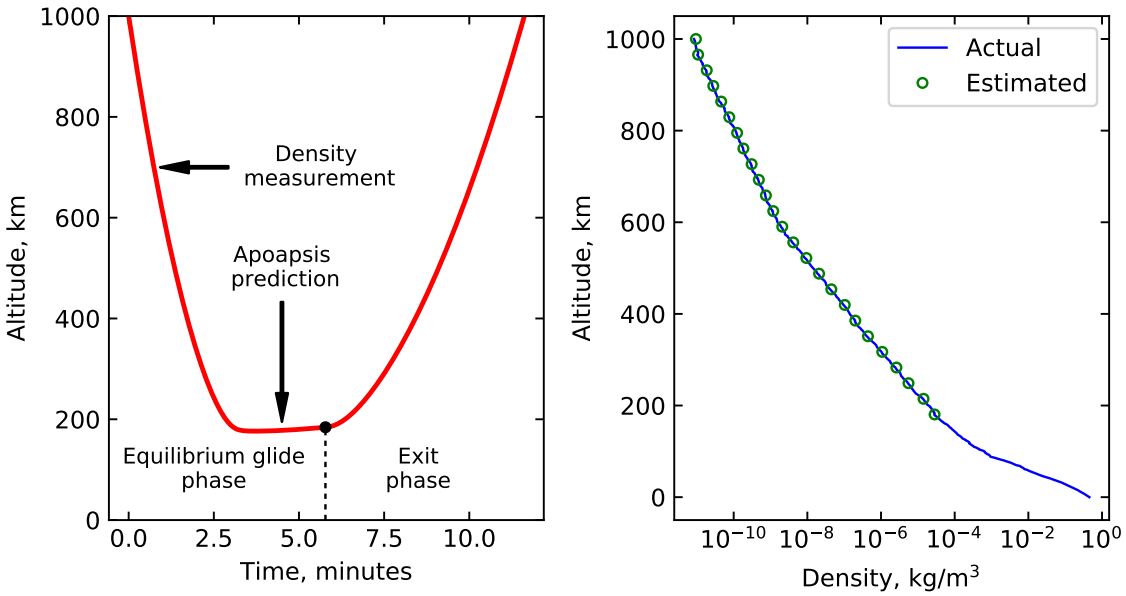

Figure 4. (Left): Altitude history of the aerocapture maneuver showing the equilibrium glide phase and exit phase of the guidance algorithm. (Right): Comparison of an actual perturbed random profile from Neptune-GRAM and estimated density profile from measured vehicle acceleration.

A key feature of the guidance algorithm proposed in the present work is the on-board density estimation during the descending leg of the aerocapture maneuver. The vehicle uses the accelerometer measurement to estimate the atmospheric density during the equilibrium glide phase till the minimum altitude is reached.

$$\rho_{\text{est}} = \frac{2ma_{\text{drag}}}{\kappa SC_Dv^2} \tag{4}$$

where, ρ_{est} is the estimated density, $a_{\text{drag.}}$ is the measured drag acceleration, S is the vehicle reference aerodynamic area, and C_D is the drag coefficient. To simplify the analysis, the present study assumes the drag deceleration is approximately equal to the total measured acceleration a_{meas} due to both lift and drag combined i.e. $a_{\text{drag}} \approx a_{\text{meas}}$. The error in density estimation due to the approximation was less than 15% for a vehicle with L/D = 0.4. We use a correction scale factor κ ranging from 1.05 to 1.15 to minimize the error between the actual and estimated density, and can be adjusted for the entry conditions, vehicle parameters, and target apoapsis. For a vehicle with L/D = 0.4 entering at 30.5 km/s for aerocapture, Fig. 4 shows the comparison of actual and estimated density profiles with κ = 1.10. Potential sources of error in the density measurement such as noise in the accelerometer reading, uncertainty in vehicle mass, aerodynamics and speed are not considered in the present study. Such errors are likely to degrade the accuracy of the density estimation slightly, and additional study is recommended to investigate the effect of noise, response time, and computational cost of constructing a reliable density function using available on-board computing resources.

While onboard density estimation has been proposed by many studies addressing aerocapture at Mars,[28–30] its application to Neptune aerocapture has not been studied. Using the onboard measured density profile significantly improves the guidance performance as compared to using a predetermined density profile. Using a preset density profile could result in erroneous prediction of the atmospheric exit conditions by the guidance algorithm. Onboard density estimation is of crucial importance to aerocapture at Neptune due to low theoretical corridor width compared to Mars or Titan. Encountering higher than expected density atmosphere could result in failure due to undershooting of planned apoapsis, and less dense atmosphere can result in apoapsis overshoot. Worst case scenarios involving low density atmosphere can result in the spacecraft not getting captured. The proposed guidance scheme allows the vehicle to accurately achieve the desired apoapsis within acceptable error even with worst-case atmospheric uncertainties as shown in the performance analysis section.

Once a predetermined altitude rate threshold is exceeded, the vehicle starts predicting its apoapsis altitude at atmospheric exit using full lift up. The prediction is done by numerically integrating the equations of motion using the density profile measured during the descending leg of the aerocapture maneuver as shown in Fig. 4. When the predicted apoapsis altitude at exit is sufficiently close to the desired value, the exit phase is initiated and the vehicle pulls out of the atmosphere with full lift up for the remainder of the atmospheric flight. Density pockets or other atmospheric phenomena not accounted for in Neptune-GRAM may be a concern for aerocapture vehicles. Density pockets have been observed in Earth's atmosphere during shuttle reentry flights.[31] A case for concern would be if the density pocket is localized, and not encountered by the vehicle during the descending leg but only during the ascending leg resulting in erroneous apoapsis prediction. Future studies can investigate the possibility of the magnitude and spatial extent of density pockets in ice giant atmospheres and its effect of aerocapture performance.

The bank angle commanded to target the desired apoapsis will result in an out-of-plane force component for bank angles other than 0° (lift-up) or 180° (lift-down). The out-of-plane force component will cause the inclination to change as the vehicle flies through the atmosphere. Since bank angle is the only control available to target both the apoapsis at exit and the inclination, the strategy adopted is to perform bank angle reversals when the inclination exceeds prescribed bounds.[27] Because the maximum roll rate is limited, the vehicle will take a few seconds to complete the roll reversal and lead to some error in apoapsis targeting. The present study focuses only on the apoapsis

targeting and leaves the inclination unconstrained for simplicity. The worst case inclination errors are likely only a few degrees during the aerocapture maneuver. Inclination errors from the atmospheric pass can be corrected using an apo-twist maneuver and may be combined with the periapse raise maneuver. Future studies will include inclination targeting in the proposed guidance scheme, and analyze its effect on apoapsis targeting accuracy for various vehicle roll rates.

PATHFINDER PROBE CONCEPT

The present study investigated the option of sending a pathfinder entry probe into Neptune atmosphere several weeks ahead of the main aerocapture vehicle reaching the atmospheric entry interface. The objective of the pathfinder probe is to measure the in-situ atmospheric profile and thus reduce the uncertainty in atmospheric profile prior to the aerocapture vehicle arriving at Neptune. Before the discussion of the pathfinder probe concept, it is insightful to discuss the "targeting problem" for aerocapture to illustrate the combined effect of navigation and atmospheric uncertainties. The targeting problem refers to the selection of a nominal target entry flight path angle (EFPA) for the aerocapture maneuver. Several weeks ahead of entering Neptune, the approach navigation maneuvers will target an aim point on the B-plane to allow the spacecraft to reach the atmospheric interface at the selected nominal EFPA.

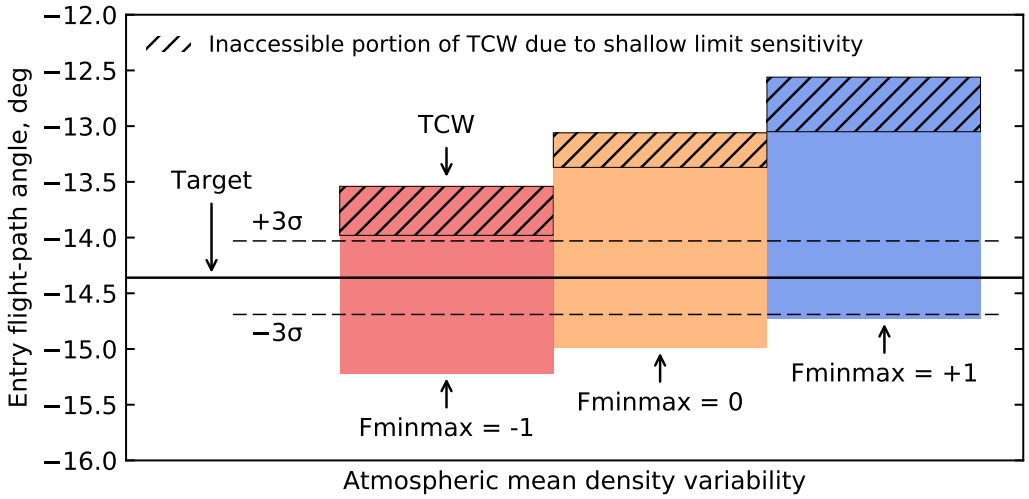

Figure 5. Schematic illustrating the combined effect of navigation and atmospheric uncertainties on target entry-flight path angle (EFPA) selection. The red, orange, and blue blocks show the theoretical aerocapture entry corridor for minimum, nominal, and maximum density atmospheric profiles. A portion of the corridor near the shallow end is hatched out due to risk of escape (even though it is theoretically feasible). The rest of the corridor is called "usable" corridor. The target EFPA should be chosen such that: 1) in the event of minimum density atmosphere (Fminmax = -1), +3σ (shallow side) delivery error is still within the usable corridor. This ensures that the vehicle is not prone to escape in the event of atmospheric density being at its lowest. 2) in the event of maximum density (Fminmax = +1), -3σ (steep side) delivery error will is within the usable corridor. If the -3σ line crosses below the usable corridor for Fminmax = +1, it implies the vehicle risks undershooting the target capture orbit. For the case shown here, the 3σ delivery errors are just small enough to fit within the corridor bounds for minimum and maximum density atmospheres. The margins against escape and undershoot are small.

The Theoretical Corridor Width (TCW) is bounded by the shallowest and steepest acceptable

EFPA for aerocapture. If the vehicle enters steeper it risks undershooting the target apoapsis or crashing into the planet, and if the vehicle enters shallower the vehicle risks overshooting the target apospsis or not getting captured. Figure 5 shows the TCW for a vehicle with L/D = 0.4 entering Neptune's atmosphere prograde at the equator at a planet-relative speed of 30.5 km/s for Fminmax = -1, 0, and +1. These values of Fminmax correspond to the minimum, average, and maximum expected mean density profiles from Neptune-GRAM. Theoretically, if the vehicle enters at any EFPA within the TCW the guidance algorithm can command the appropriate bank angle profile to achieve the desired exit conditions. However, simulations indicate that entry near the shallow limit of the corridor which requires almost full lift-down for the entire trajectory are very sensitive to disturbances and such trajectories are not flyable in practice due to the risk of flyaway without getting captured. The hatched regions in Fig. 5 show the portion of the corridor rendered inaccessible due to the sensitivity of trajectories near the shallow limit using the guidance algorithm described earlier and parameters listed in Appendix A. Thus the usable corridor for Neptune aerocapture is smaller than the theoretical corridor. Though the width of the corridor is not very sensitive to Fminmax, the shallow and steep bounds of the usable corridor change significantly based on the mean density profile and leads to the targeting problem. The selected nominal EFPA should be such that the $\pm 3\sigma$ navigation uncertainty should fall within the usable corridor for the entire range of mean density profile uncertainties. Targeting the selected nominal EFPA allows the aerocapture vehicle to achieve the desired exit conditions for any mean atmospheric profile within the specified uncertainty.

In the present study, it is seen that a 3σ EFPA uncertainty of 0.33 (Table 2) shown in Fig. 5 is sufficient to accommodate the entire range of mean density profiles from Fminmax = -1 to +1, though the safety margins over 3σ are small. The safety margin on the shallow side is indicated by the small gap between the $+3\sigma$ EFPA boundary and the shallow limit of the usable corridor for Fminmax = -1. If the vehicle encounters the lowest density atmosphere (Fminmax = -1), and the EFPA falls outside $+3\sigma$, then the vehicle risks not getting captured. The safety margin on the steep side is indicated by the difference between the -3σ EFPA boundary and the steep limit of the usable corridor for Fminmax = +1. If the vehicle encounters the highest density atmosphere (Fminmax = +1), and the EFPA falls outside -3σ, then the vehicle risks undershooting the apoapsis or burning up in the atmosphere.

Simulations performed in the present study indicate that off-nominal EFPA outside $+3\sigma$ are likely to flyaway without getting captured, while off-nominal EFPA outside -3σ will only likely result in undershoot of apoapsis but certainly not crash into the planet. The flyway case will almost certainly lead to loss of mission, while the apoapsis undershoot can be corrected using propulsive maneuvers and Triton gravity assists during the course of the mission. It is recommended to bias the target EFPA towards the steep side of the usable corridor to provide sufficient safety margin against the flyaway scenario for minimum density atmosphere, even if the -3σ EFPA bound falls outside the usable corridor for the maximum density atmosphere. Two possible options to increase the safety margin are: 1) decrease the navigation uncertainties further, and 2) reduce the atmospheric uncertainties. The pathfinder probe concept aims to use the second option of reducing atmospheric uncertainties to improve the safety margin against accidental escape.

The concept of operations for the pathfinder probe is as follows. Several weeks ahead of the main aerocapture vehicle reaching Neptune, an atmospheric entry probe is released from the main spacecraft. The carrier spacecraft also releases two CubeSats on a flyby trajectory with their arrival timed so as to act as a data relay from the probe during entry. The probe coasts to Neptune, while the main spacecraft performs trajectory correction maneuvers (TCM) such that it arrives at entry

interface for aerocapture a few weeks after the probe entry. The probe measures the density in-situ (from accelerometer measurement), along with atmospheric structure and composition. The data is relayed to the main spacecraft via the CubeSats, which in turn relays the data back to Earth. The present study hypothesizes that the in-situ data when coupled with improved atmospheric models and prior ground based observation campaigns can significantly reduce the uncertainty in mean density profile to be encountered by the main aerocapture vehicle.

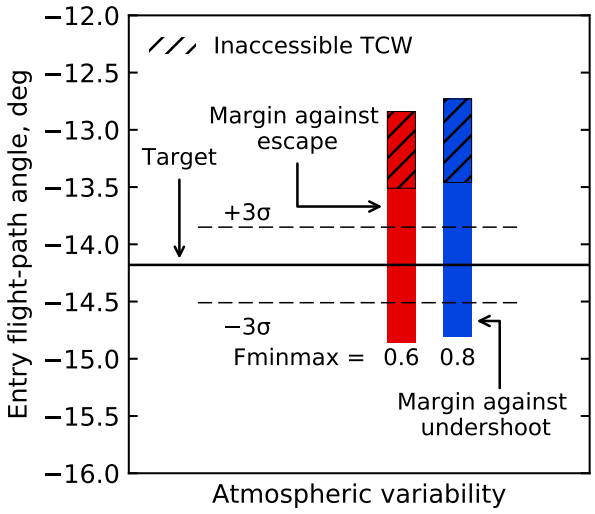

Figure 6. Improved margins against escape and undershoot from reduced atmospheric uncertainty. The smaller range of atmospheric density uncertainty compared to Fig. 5 allows greater margins against escape and undershoot.

While there is little doubt that data from a pathfinder probe can reduce the atmospheric uncertainty, quantification of the uncertainty reduction is not possible at the level of the study. For illustration, the present study assumes that the pathfinder probe data is able to constrain the atmospheric uncertainties such that $0.6 \leq \text{Fminmax} \leq 0.8$ instead of the full range of Fminmax from -1 to +1. With the reduced uncertainty in Fminmax, the target EFPA can be chosen so as to provide sufficient margin against escape above 3σ in the case of low density atmosphere, and against undershoot in the case of high density atmosphere as shown in Fig. 6. The pathfinder probe allows optimal selection of the target EFPA to minimize the risk of accidental escape or apoapsis undershoot. The present study finds that a pathfinder probe is not necessary for aerocapture at Neptune for if the navigation accuracy in Tab. 2 can be realized, and the atmospheric uncertainties are within those provided by Neptune-GRAM. However, if available, the pathfinder probe can improve the safety margin for aerocapture against escape and undershoot scenarios. The study finds that the pathfinder probe is a feasible option and future Neptune aerocapture studies can further investigate the concept. Constraints on the timing of probe and CubeSat release, data transmission from the probe to the CubeSats, propulsive ΔV associated with deflection maneuvers, the time available for data analysis and command upload to spacecraft for targeting the optimal EFPA are recommended for investigation by future studies.

Inclusion of a pathfinder probe (in addition to a potential main probe) adds cost, risk, and complexity to the mission architecture. The possibility of the pathfinder probe failing to accomplish its mission should be considered, due to entry probe failure, loss of data etc. Loss of the pathfinder

probe cannot be a single point failure for the main aerocapture vehicle and should be capable of performing the maneuver with sufficient safety margin even if the data from the pathfinder probe is not available. The pathfinder probe is recommended to be used as an option to enhance the safety margin for aerocapture, but not as mission critical component for ice giant mission architectures.

PERFORMANCE ANALYSIS

Monte Carlo analysis is used to quantify the vehicle performance in the presence of combined navigation, atmospheric, and aerodynamic uncertainties. Nominal values of the parameters used and the associated uncertainties are listed in Table 4. The target entry flight-path angle is chosen based on the discussion earlier concerning the targeting problem in the section on pathfinder probe. For arrival V_∞ = 20 km/s of the reference interplanetary trajectory, the planet/atmosphere relative entry speed can range from 27.8 km/s for equatorial prograde entry to 33.3 km/s for retrograde entry. The location and width of the entry corridor changes as a function of the planet-relative entry speed and hence must be accounted for in aerocapture guidance analysis. For simplicity, the present analysis uses an entry speed of 30.5 km/s which is midway between the two limiting values. At atmospheric exit, the inertial speed is computed assuming prograde equatorial orientation of the planet-relative velocity vector and the apoapsis altitude is computed using the inertial speed. Atmospheric mean density profile uncertainties and random high frequency perturbations are used from Neptune-GRAM. Aerodynamic uncertainties were not estimated in the present study, but a nominal 10% dispersion is used. Three sets of simulations were performed: 1) maximum range of Fminmax, 2) reduced atmospheric uncertainty, and 3) very low atmospheric uncertainty.

Maximum Range of Fminmax

The maximum atmospheric uncertainty case assumes that no improvement is available over data from Neptune-GRAM and the vehicle must accommodate the full range of Fminmax from -1 to +1.

Table 4. Monte Carlo uncertainties

Category	Variable	Nominal	$\pm 3\sigma$ or [min,max] or other	Distribution
Navigation	Entry flight-path angle	-14.48°	$\pm$ 0.33°	Normal
Atmosphere	Fminmax	-	[-1, +1]	Uniform
	Mean density uncertainty	0	3σ from Neptune-GRAM	Normal
	High frequency perturbation (rpscale = 1)	-	-	Random
Aerodynamics	L/D	0.40	$\pm$0.04	Normal

Vehicle parameters used for the simulation are β = 200 kg/m^2, L/D = 0.4. C_D = 1.59, and nose radius R_N = 1.0 m. The target apoapsis altitude is 400,000 km, with an apoapsis error tolerance of 10,000 km used by the guidance algorithm. The apoapsis prediction is initiated when the altitude rate exceeds -500 m/s and a guidance frequency of 2 Hz (i.e. new bank angle commands are generated at 2 Hz) is used for the equilibrium glide phase. The onboard density estimation assumes perfect knowledge of the total measured acceleration and other vehicle parameters and computes the density once during every guidance cycle. Guidance gain parameters used in the simulation are described in Appendix A. If the guidance algorithm predicts an apoapsis altitude lower than the target value, the equilibrium glide phase is terminated immediately and the vehicle flies full lift-up. Higher guidance frequency can improve the apoapsis targeting, albeit at the cost of greater on-board computing requirements. Vehicle state parameters such as altitude, latitude and longitude, heading,

altitude rate, speed used by the guidance scheme will have uncertainties associated with inertial sensors but for the present study are assumed to be known perfectly. We choose a density correction factor $\kappa = 1.06$ (based on simulation data) to minimize the apoapsis targeting errors. The maximum allowed roll rate is 30 degrees/sec. Orbit inclination is left unconstrained in the present study for simplicity. Bank reversals to track the target inclination will take a few seconds to complete and affect the apoapsis targeting accuracy, but is not expected to degrade the performance significantly.

A high-fidelity 3-DoF simulation including gravity zonal harmonics up to J_4, aerodynamic forces, Corioils force, and centrifugal force is used to simulate the trajectory of a spacecraft flying in the vicinity of an oblate, rotating planet. The simulation uses an outer loop to propagate the actual vehicle trajectory, and an inner loop to simulate the guidance scheme. 5000 simulated aerocapture trajectories were run, and the results are used to assess aerocapture guidance performance at Neptune using a blunt-body aeroshell. All of the 5000 cases captured successfully with 98.8% of the cases achieving apoapsis within $\pm$50,000 km of the target apoapsis (= 400,000 km). Figure 7 shows the histogram of the achieved apoapsis altitude and the dispersion in apoapsis vs. periapsis altitude. Trajectory #3585 resulted the lowest apoapsis altitude of 197,944 km which is attributed to high mean density (Fminmax = +1.0), $+1.29\sigma$ density variation about the mean profile, and steep EFPA = -14.70 ($+2\sigma$) along with the effect of random density perturbations.

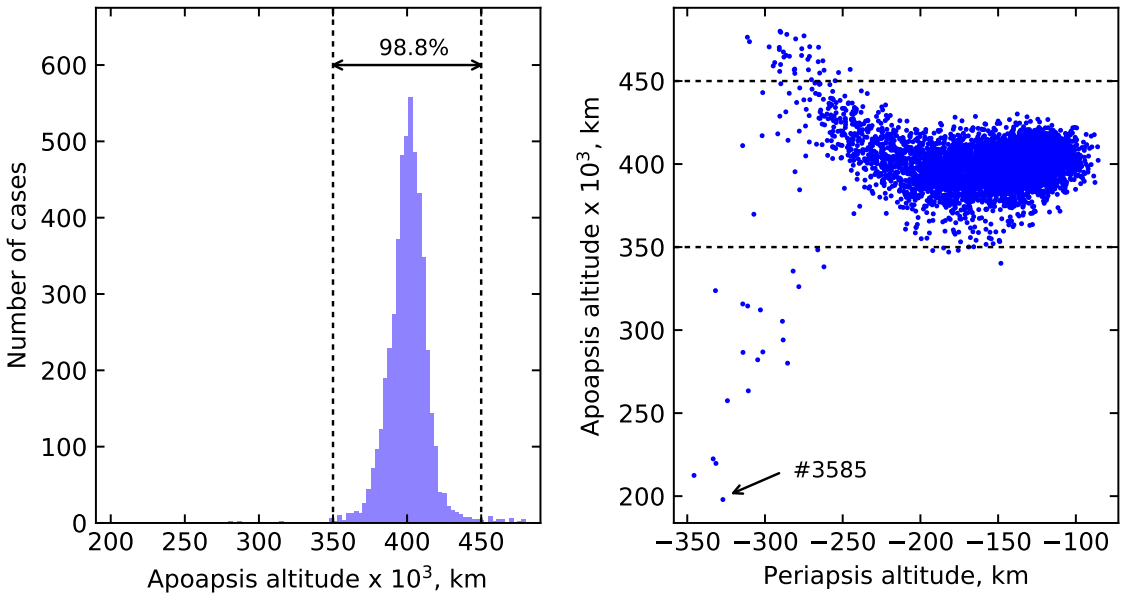

Figure 7. (Left): Histogram of achieved apoapsis altitude for maximum range of Fminmax. 98.8% of the cases achieved apoapsis within $\pm$ 50,000 km of the target. (Right): Apoapsis altitude vs. periapsis altitude. A small fraction of cases resulted in slight overshoot of the target apoapsis (above 450,000 km) while a larger fraction resulted in apoapsis undershoot (below 350,000 km). This is attributed to the fact that the safety margins were rather small as shown in Fig. 5. The target EFPA is slightly biased towards the steep side of the corridor to reduce the risk of escape, but this results in some cases undershooting the target apoapsis. Apoapsis undershoot can be corrected using propulsive manuevers and is a more favorable outcome compared to escape scenarios from which the spacecraft very likely cannot be recovered.

Figure 8 shows the dispersion in peak deceleration and peak stagnation-point heat rate. The stagnation point heat-rate is the sum of convective and radiative heating rates computed using en-

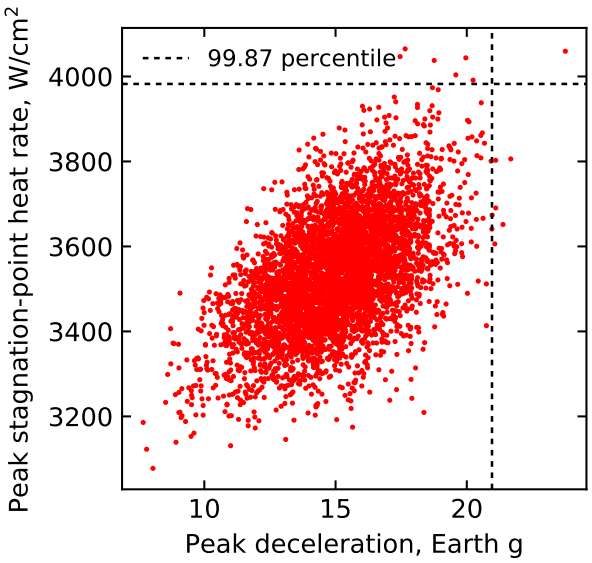

Figure 8. Peak deceleration vs. peak stagnation-point heat rate for maximum range of Fminmax. The 99.87 percentile peak deceleration load is 21g which is an important parameter for vehicle structural design, and instrument qualification. The 99.87 percentile peak stagnation-point heat rate is 3,982 W/cm^2 which is within the capability of HEEET TPS material. We note these are preliminary estimates and higher fidelity studies are required to validate the heating predictions.

gineering correlations.[18] The 99.87 percentile peak deceleration load is 21g and is an important parameter for aeroshell structural design and science instrument design. The 99.87 percentile peak stagnation-point heat rate is 3,982 W/cm^2, an important parameter for TPS material selection and qualification. It is noted that the engineering correlations used in the present study have limited accuracy, and future studies using high-fidelity CFD models are required to validate the heating predictions and TPS performance characterization under the expected aerothermal environments. Table 5 summarizes the percentiles for various parameters from the Monte Carlo simulation. The 99.87 percentile propulsive ΔV requirement for periapsis raise and apoapsis correction is 396 m/s.

For the maximum range of Fminmax, the EFPA is slightly biased towards the steep side to ensure sufficient margin against accidental flyaway. As seen in Fig. 5 this results in the lack of or negative margin against undershoot for the high density scenario and is the reason for some trajectories undershooting the apoapsis. The apoapsis undershoot can be corrected using propulsive maneuvers within reasonable ΔV budget, whereas the ΔV required to recover the spacecraft from an accidental escape scenario is prohibitively high.

Table 5. Statistics from Monte Carlo simulation with full range of Fminmax

Parameter	Minimum	0.13 percentile	Mean	99.87 percentile	Maximum
Apoapsis altitude, km	197,944	281,089	400,288	472,207	480,013
Peak deceleration, Earth g	7.67	8.77	14.97	20.96	23.75
Peak heat rate, W/cm^2	3,077	3,166	3,534	3,982	4,064
Periapsis raise ΔV, m/s	89.54	90.65	101.55	141.08	186.91
Apoapsis correction ΔV, m/s	0.01	0.02	16.10	255.13	581.52
Total propulsive ΔV, m/s	99.93	100.47	117.66	396.21	768.44

Reduced Atmospheric Uncertainty

To investigate the effect of reduced atmospheric uncertainty from potential ground based observations and atmospheric modelling efforts, the simulation is run with -0.5 $\leq$ Fminmax $\leq$ +0.5, and rpscale = 0.5 indicating lower high frequency density perturbation amplitudes. Other simulation parameters are the same as mentioned in Table 4. All cases captured successfully and the dispersion in apoapsis altitude is smaller compared to the case with the full range of Fminmax. Figure 9 shows that 99.8% of the cases achieved apoapsis within $\pm$50,000 km of the target, compared to 98.8% for the case with full range of Fminmax. Only one case (#316) resulted in apoapsis altitude outside below the 350,000 km bound which is attributed to high density atmosphere (Fminmax = +0.5), steep EFPA = -14.83° (+3.2σ), low L/D = 0.367 (-2.5σ). The combined probability of a +3.2σ EFPA error and -2.5σ L/D value is approximately 1 in 50,000. Despite the low probability of such an event, a propulsive maneuver of 524 m/s can still correct the apoapsis and achieve the desired orbit. Table 6 summarizes the percentiles for various parameters from the Monte Carlo simulations for the reduced atmospheric uncertainty case. The 99.87 percentile total propulsive ΔV is 175.87 m/s compared to 396.21 m/s for the case with full range of Fminmax. The results show that apoapsis errors are smaller compared to -1 $\leq$ Fminmax $\leq$ +1, and hence the total propulsive ΔV requirement is lower. The lower ΔV requirement can be used to lower the safety margin on propellant carried, or allow more propellant to be used for moon tours and satellite flyby targeting during the science mission.

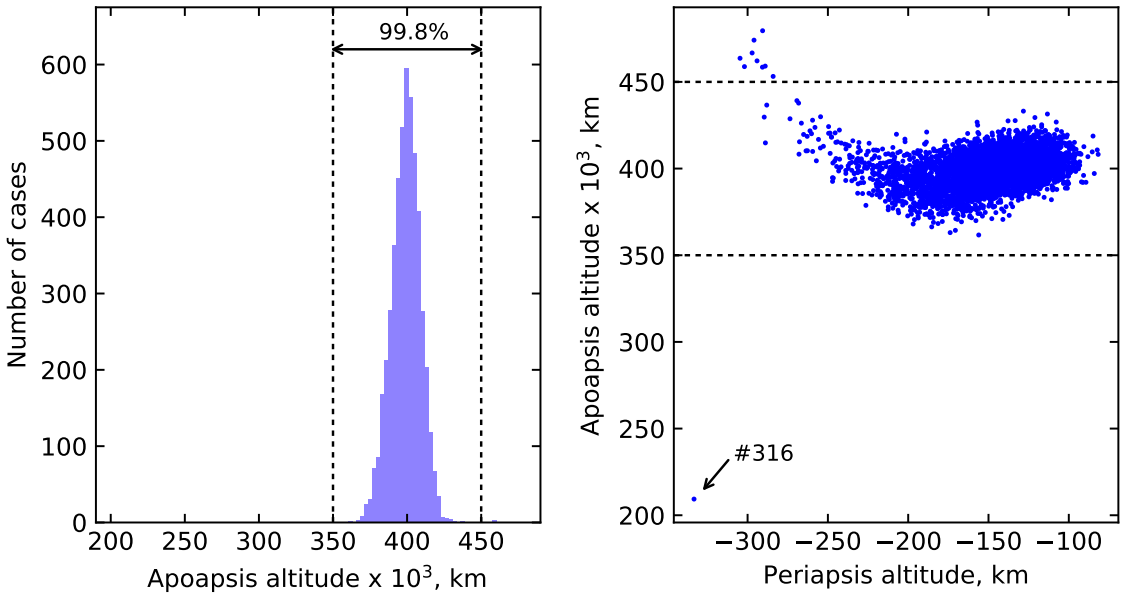

Figure 9. Results for reduced atmospheric uncertainty case; -0.5 $\leq$ Fminmax $\leq$ +0.5.

Very Low Atmospheric uncertainty

To illustrate the effect of very low atmospheric uncertainty as may be possible using data from a pathfinder probe, the simulation is run with 0.6 $\leq$ Fminmax $\leq$ 0.8, and rpscale = 0.5. Based on the lower atmospheric uncertainty, we choose the target EFPA to be -14.16° to allow sufficient margin against escape and undershoot as indicated in Fig. 6.

Table 6. Statistics with reduced atmospheric uncertainty; -0.5 $\leq$ Fminmax $\leq$ +0.5, rpsacle = 0.5

Parameter	Minimum	0.13 percentile	Mean	99.87 percentile	Maximum
Apoapsis altitude, km	209,330	368,619	399,342	458,660	479,518
Peak deceleration, Earth g	9.41	10.01	14.82	19.77	20.31
Peak heat rate, W/cm^2	3,195	3,212	3,497	3,778	3,872
Periapsis raise ΔV, m/s	89.64	93.33	101.51	109.57	179.45
Apoapsis correction ΔV, m/s	0.00	0.03	12.43	81.91	524.23
Total propulsive ΔV, m/s	100.15	100.52	113.94	175.87	703.71

Table 7. Statistics with very low atmospheric uncertainty; 0.6 $\leq$ Fminmax $\leq$ 0.8, rpsacle = 0.5

Parameter	Minimum	0.13 percentile	Mean	99.87 percentile	Maximum
Apoapsis altitude, km	366,475	376,427	401,673	426,254	429,674
Peak deceleration, Earth g	8.12	9.12	12.32	15.97	16.56
Peak heat rate, W/cm^2	2,962	3,043	3,284	3,506	3,538
Periapsis raise ΔV, m/s	94.14	94.79	99.89	106.78	109.04
Apoapsis correction ΔV, m/s	0.00	0.01	10.64	41.07	57.02
Total propulsive ΔV, m/s	99.19	99.58	110.52	145.52	166.06

100% of the cases achieved apoapsis within 350,000 and 450,000 km as shown in Fig. 10 . The results show that a pathfinder probe can be used to significantly improve the accurate apoapsis targeting. The improved safety margin may be used to accommodate density pockets or other density anomalies which may be present but are not easily predictable. Table 7 summarizes the results for the very low atmospheric uncertainty case. The 99.87 percentile total propulsive ΔV required is 145.52 m/s which is only a marginal improvement over 175.87 m/s with -0.5 $\leq$ Fminmax $\leq$ +0.5. The present study recommends that future studies investigate if near-term efforts using observations and numerical models can lower the atmospheric uncertainties such that -0.5 $\leq$ Fminmax $\leq$ +0.5. If atmospheric uncertainties cannot be reduced to the extent required for acceptable apoapsis targeting errors, a pathfinder probe is likely a feasible option to ensure adequate safety margins.

CONCLUSIONS

Interplanetary trajectories with high arrival V_∞ allows the vehicle L/D requirement to be lowered and also allows significantly shorter time of flight for missions to Neptune. Approach navigation analysis using state-of-the-art techniques have shown that delivery errors can be reduced compared to previous estimates. A guidance algorithm using bank angle modulation and on-board density estimation has been developed and is shown to be able to guide the spacecraft to the desired exit conditions even with large uncertainties in atmospheric density. Monte Carlo simulation is used to test guidance performance with combined navigation, atmospheric, and aerodynamic uncertainties. One hunded percent of the cases captured successfully and 98.8% of the cases achieved apoapsis within $\pm$50,000 km of the target with the full range of Fminmax. For reduced atmospheric uncertainty from potential ground based observations and modeling, 99.8% cases achieved apoapsis within $\pm$50,000 km of the target. For a hypothetical very low atmospheric uncertainty scenario, as is likely to be the case if pathfinder probe is available, 100% cases achieved apoapsis within $\pm$50,000 km of the target. The combination of fast arrival trajectory, reduced navigation uncertainties, and improved guidance scheme is shown to allow a heritage blunt-body aeroshell with L/D = 0.4 to successfully perform aerocapture at Neptune even with worst case atmospheric uncertainties.

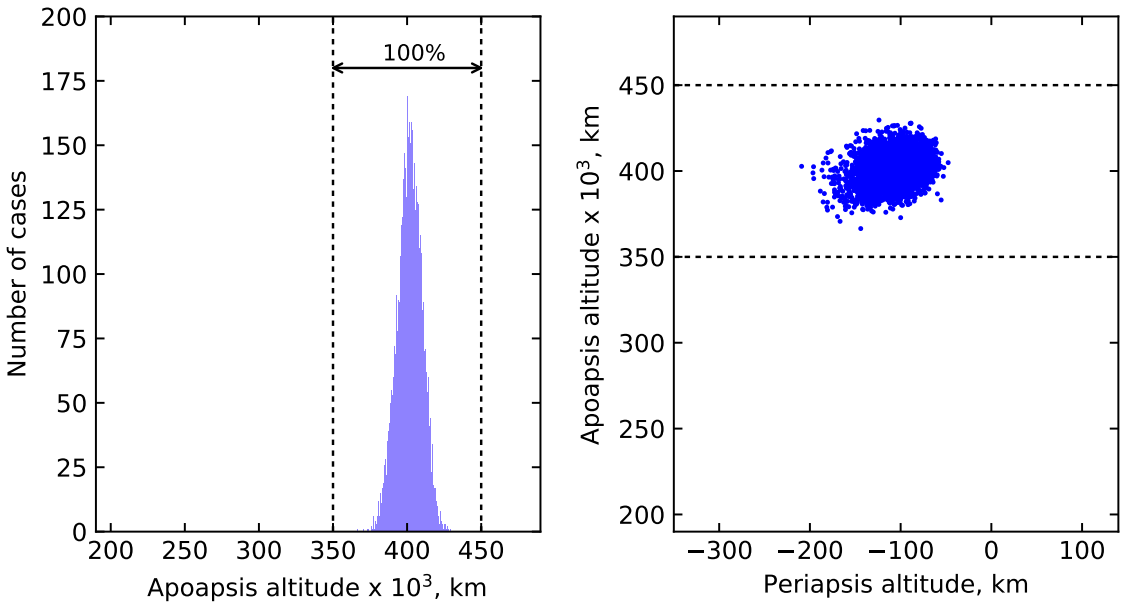

Figure 10. Results for reduced atmospheric uncertainty case; 0.6 $\leq$ Fminmax $\leq$ 0.8.

ACKNOWLEDGMENTS

The authors acknowledge Dr. Anastassios Petropoulos at the NASA Jet Propulsion Lab and Dr. Nitin Arora, formerly at the NASA Jet Propulsion Lab for providing the interplanetary trajectory data used in this study. The research described in this report was carried out at Purdue University and has been supported in part by the Jet Propulsion Laboratory, California Institute of Technology, under subcontract 1578703.

REFERENCES

[1] M. K. Lockwood, K. T. Edquist, B. R. Starr, B. R. Hollis, G. A. Hrinda, R. W. Bailey, *et al.*, "Aerocapture Systems Analysis for a Neptune Mission," Tech. Rep. NASA/TM-2006-214300, NASA Langley Research Center, Langley, VA, 2006.

[2] T. R. Spilker, "Significant Science at Titan and Neptune from Aerocaptured Missions," *Planetary and Space Science*, Vol. 53, No. 5, 2005, pp. 606–616.

[3] A. P. Ingersoll and T. R. Spilker, "A Neptune Orbiter with Probes Mission with Aerocapture Orbit Insertion," *Progress in Astronautics and Aeronautics: NASA Space Science Vision Missions*, Vol. 224, 2008, pp. 81–113.

[4] T. R. Spilker, M. Adler, N. Arora, P. M. Beauchamp, J. A. Cutts, M. M. Munk, *et al.*, "Qualitative Assessment of Aerocapture and Applications to Future Missions," *Journal of Spacecraft and Rockets*, Nov. 2018, pp. 1–10.

[5] R. Carpenter, "Aeroasist Flight Experiment," Tech. Rep. ASE 396, Texas Space Grant Consortium, Austin, TX, 1992.

[6] P. Wercinski, W. Henline, H. Tran, F. Milos, P. Papadopoulos, Y.-K. Chen, *et al.*, "Trajectory, Aerothermal Conditions, and Thermal Protection System Mass for the Mars 2001 Aerocapture Mission," *35th Aerospace Sciences Meeting and Exhibit*, Reno, NV, 1997, p. 472, 10.2514/6.1997-472.

[7] R. Powell, "Numerical Roll Reversal Predictor Corrector Aerocapture and Precision Landing Guidance Algorithms for the Mars Surveyor Program 2001 Missions," *23rd Atmospheric Flight Mechanics Conference*, Boston, MA, AIAA, 1998, p. 4574, 10.2514/6.1998-4574.

[8] C. Cazaux, F. Naderi, C. Whetsel, D. Beaty, B. Gershman, R. Kornfeld, *et al.*, "The NASA/CNES Mars Sample Return—A Status Report," *Acta Astronautica*, Vol. 54, No. 8, 2004, pp. 601–617, 10.1016/j.actaastro.2003.07.001.

[9] A. Keys, J. Hall, D. Oh, and M. Munk, "Overview of a Proposed Flight Validation of Aerocapture System Technology for Planetary Missions," *42nd AIAA/ASME/SAE/ASEE Joint Propulsion Conference & Exhibit*, Sacramento, CA, AIAA, 2006, p. 4518, 10.2514/6.2006-4518.

[10] J. L. Hall, M. A. Noca, and R. W. Bailey, "Cost-Benefit Analysis of the Aerocapture Mission Set," *Journal of Spacecraft and Rockets*, Vol. 42, No. 2, 2005, pp. 309–320, 10.2514/1.4118.

[11] M. K. Lockwood, B. R. Starr, J. W. Paulson, D. A. Kontinos, Y. K. Chen, Laub, *et al.*, "Systems Analysis for a Venus Aerocapture Mission," Tech. Rep. NASA/TM-2006-214291, NASA Langley Research Center, Hampton, VA, 2006.

[12] H. S. Wright, D. Y. Oh, C. H. Westhelle, J. L. Fisher, R. E. Dyke, K. T. Edquist, J. L. Brown, H. L. Justh, and M. M. Munk, "Mars Aerocapture Systems Study," Tech. Rep. NASA/TM-2006-214522, NASA Langley Research Center, Hampton, VA, 2006.

[13] M. K. Lockwood, E. M. Queen, D. W. Way, R. W. Powell, K. Edquist, B. W. Starr, *et al.*, "Aerocapture Systems Analysis for a Titan Mission," Tech. Rep. NASA/TM-2006-214273, NASA Langley Research Center, Hampton, VA, 2006.

[14] Y. Lu and S. J. Saikia, "Feasibility Assessment of Aerocapture for Future Titan Orbiter Missions," *Journal of Spacecraft and Rockets*, Vol. 55, 9 2018, pp. 1125–1135, 10.2514/1.A34121.

[15] B. Starr, C. Westhelle, and J. Masciarelli, "Aerocapture Performance Analysis for a Neptune-Triton Exploration Mission," *AIAA Atmospheric Flight Mechanics Conference and Exhibit*, Providence, RI, 2004, p. 4955.

[16] J. Masciarelli, C. Westhelle, and C. Graves, "Aerocapture Guidance Performance for the Neptune Orbiter," *AIAA Atmospheric Flight Mechanics Conference and Exhibit*, Providence, RI, 2004, p. 4954.

[17] M. D. Hofstadter, A. Simon, K. Reh, and J. Elliot, "Ice Giants Pre-Decadal Study Final Report," Tech. Rep. JPL D-100520, NASA, Pasadena, CA, 2017.

[18] B. Bienstock, D. Atkinson, S. Atreya, P. Mahaffy, K. Baines, M. Wright, *et al.*, "NASA Vision Mission Neptune Orbiter with Probes," Tech. Rep. Contract No. NNH04CC41C, NASA, 2005.

[19] A. B. Sergeyevsky, G. C. Snyder, and R. A. Cunniff, "Interplanetary Mission Design Handbook. Volume 1, part 2: Earth to Mars ballistic mission opportunities, 1990-2005," Tech. Rep. JPL-PUBL-82-43-VOL-1-PT-2, Pasedena, CA, 1983.

[20] E. Stone and E. Miner, "The Voyager 2 Encounter with the Neptunian System," *Science*, Vol. 246, No. 4936, 1989, pp. 1417–1421, 10.1126/science.246.4936.1417.

[21] C. Justus, A. Duvall, and V. Keller, "Atmospheric Models for Aerocapture," *40th AIAA/ASME/SAE/ASEE Joint Propulsion Conference and Exhibit*, Fort Lauderdale, FL, AIAA, 2004.

[22] A. Duvall, C. Justus, and V. Keller, "Global Reference Atmospheric Model (GRAM) Series for Aeroassist Applications," *43rd AIAA Aerospace Sciences Meeting and Exhibit*, Reno,NV, AIAA, 2005, 10.2514/6.2005-1239.

[23] H. Justh, "Neptune-GRAM 2004 Documentation," 2004.

[24] C. Justus, A. Duvall, and D. Johnson, "Engineering-level Model Atmospheres for Titan and Neptune," *39th AIAA/ASME/SAE/ASEE Joint Propulsion Conference and Exhibit*, Huntsville, AL, 2003, p. 4803, 10.2514/6.2003-4803.

[25] E. R. Hillje, "Entry Flight Aerodynamics from Apollo Mission AS-202," Tech. Rep. NASA TN D-4185, Washington D. C., October, 1967.

[26] D. W. Way, R. W. Powell, A. Chen, A. D. Steltzner, A. M. San Martin, P. D. Burkhart, *et al.*, "Mars Science Laboratory: Entry, Descent, and Landing System Performance," *Aerospace Conference, 2007 IEEE*, Big Sky, MT, IEEE, March 3–10, 2007, pp. 1–19, 10.1109/AERO.2007.352821.

[27] C. Cerimele and J. Gamble, "A Simplified Guidance Algorithm for Lifting Aeroassist Orbital Transfer Vehicles," *23rd Aerospace Sciences Meeting*, Houston, TX, 1985, p. 348, 10.2514/6.1985-348.

[28] E. Perot and S. Rousseau, "Importance of an On-board Estimation of the Density Scale Geight for Various Aerocapture Guidance Algorithms," *AIAA/AAS Astrodynamics Specialist Conference and Exhibit*, Monterey, CA, 2002, p. 4734.

[29] J. F. Hamel and J. D. Lafontaine, "Improvement to the Analytical Predictor-Corrector Guidance Algorithm Applied to Mars Aerocapture," *Journal of Guidance, Control, and Dynamics*, Vol. 29, No. 4, 2006, pp. 1019–1022.

[30] J. Wagner, A. Wilhite, D. Stanley, and R. Powell, "An Adaptive Real Time Atmospheric Prediction Algorithm for Entry Vehicles," *3rd AIAA Atmospheric Space Environments Conference*, Honolulu, HI, 2011, p. 3200, 10.2514/6.2011-3200.

[31] L. Skalecki, C. Cerimele, and J. Gamble, "Meteorological Accuracy Requirements for Aerobraking Orbital Transfer Vehicles," *22nd Aerospace Sciences Meeting*, Houston, TX, 1984, p. 30, 10.2514/6.1984-30.

APPENDIX A: GUIDANCE PARAMETERS

The gain parameters used in the equilibrium glide phase guidance is computed based on the procedure developed by Cerimele and Gamble.[27] The vehicle altitude dynamic response can be shown to be:

$$\ddot{h} + \frac{C_L S}{m} G_{\dot{h}} \dot{h} - \frac{C_L S}{m} G_{\bar{q}} \left(\bar{q} - \bar{q}_{\text{ref}} \right) = 0 \tag{5}$$

Equation 5 can be approximated as a linear second order system by assuming $\bar{q} = ah + b$, and the system response is characterized by

$$\omega_n{}^2 = -\frac{C_L S}{m} G_{\bar{q}} a \tag{6}$$

$$2\zeta\omega_n = \frac{C_L S}{m} G_{\dot{h}} \tag{7}$$

For a vehicle with $m/C_L S$ = 500 kg/m^2, L/D = 0.4 entering Neptune atmosphere with planet-relative speed V = 30.5 km/s, EFPA = -14.38° and using full lift up, the dynamic pressure as a function of altitude is shown in Fig. 11. A linear approximation can be made for the pressure profile as the vehicle descends below 300 km, and the aerodynamic forces become significant. Using ω_n = 0.05 rad/s and ζ = 1.50, the gain parameters can be calculated to be $G_{\dot{h}}$ = 75.0 and $G_{\bar{q}}$ = 3.316. These values provided acceptable vehicle response, and was used for all simulations in the present study. For a vehicle with different $m/C_L S$, or for different entry conditions, the above procedure can be used to recalculate the gain parameters. Additional study is recommended to investigate if the gain parameters can be optimized to minimize the loss of corridor due to shallow limit sensitivity.

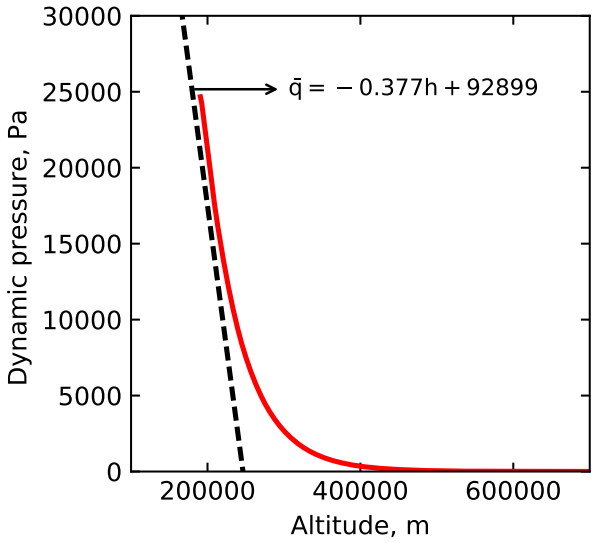

Figure 11. Actual dynamic pressure profile (solid line) and linear approximation (dashed line) of the used to calculate guidance gain parameters.